*electronics*

MDPI

*Article*

# Development of a Wideband Slotted Antenna Array with Low Profile and Low Sidelobe (Invited Paper)

**Haoyun Yuan [1], Jinkai Li [2], Zhibo Zhao [1], Zeyu Wang [2], Matteo Bruno Lodi [3], Giovanni Gugliandolo [4], Nicola Donato [4], Giovanni Crupi [5], Liming Si [1,2] and Xiue Bao [1,2,*]**

1 School of Integrated Circuits and Electronics, Beijing Institute of Technology, Beijing 100081, China
2 Tangshan Research Institute, BIT, Tangshan 063000, China
3 Department of Electrical and Electronic Engineering, University of Cagliari, 09123 Cagliari, Italy
4 Engineering Department, University of Messina, 98166 Messina, Italy
5 BIOMORF Department, University of Messina, 98125 Messina, Italy
* Correspondence: xiue.bao@bit.edu.cn

**Abstract:** In this paper, a novel multi-layered waveguide-fed slotted cavity antenna array operating in the K-band (i.e., 18–27 GHz) is presented. The antenna is composed of 64 (8 × 8) groups of 2 × 2 subarrays with low profile, and fed by a 1–64 ways waveguide corporate-feed-network. In order to obtain a low sidelobe level (SLL), the Chebyshev power distribution is introduced into the feeding network to accurately taper the power distribution among the subarrays. To realize the amplitude-tapering network, a simple T-junction, which can provide equal phase but unequal power, is used. The antenna array is analyzed and validated by using the finite element method (FEM). Simulation results demonstrate that the proposed antenna array can achieve a broad bandwidth of 21.9%, and a good gain as 29.1 dBi. Additionally, the first SLL can be as small as −28.3 dB and −20 dB in the *E*-plane and the *H*-plane, respectively. The overall size of the slotted cavity antenna array is 169.6 × 169.6 × 7.23 mm$^3$.

**Keywords:** antenna array; K-band; low sidelobe; slotted cavity array; wideband; wireless communication



**Citation:** Yuan, H.; Li, J.; Zhao, Z.; Wang, Z.; Lodi, M.B.; Gugliandolo, G.; Donato, N.; Crupi, G.; Si, L.; Bao, X. Development of a Wideband Slotted Antenna Array with Low Profile and Low Sidelobe (Invited Paper). *Electronics* **2023**, *12*, 278. https://doi.org/10.3390/electronics12020278

Academic Editors: Shuvashis Dey, Benjamin D. Braaten, Dipankar Mitra and Athanasios D. Panagopoulos

Received: 14 December 2022
Revised: 30 December 2022
Accepted: 2 January 2023
Published: 5 January 2023



## 1. Introduction

With the development of wireless communication systems, high-frequency bands are gaining increasing attention. For instance, in recent years, the K-band (i.e., 18–27 GHz) has been used in many radar and satellite communication systems [1–4]. To reduce external interference and improve communication quality, high-performance antennas, which have high gain (>25 dBi), low profile, and low sidelobe level (SLL ≤ −20 dB), are often required [5–7]. Due to the easy fabrication and integration with other circuits, planar antennas, including microstrip-based [8–10] and substrate-integrated waveguide (SIW)-based [11,12] structures, have been widely used. However, these planar antennas are obviously affected by the dielectric loss of the planar substrates at high frequencies [13,14]. To solve this problem, waveguide slot arrays with low insertion loss have been studied for achieving high-gain and low-profile engineering solutions [15–19].

Typically, a slotted waveguide antenna array is fed with a series structure [20], which is widely used due to its simpleness. However, when the size of the arrays becomes large, its long-line effect can dramatically affect its working bandwidth [21]. To solve this problem, some multi-layered slotted waveguide antenna arrays have been proposed [22–24], where a full-corporate-feed network is used. Generally, there are at least four layers, including a radiation layer, a cavity layer, a coupling layer, and a feeding layer. However, in the back cavity between the radiation layer and the coupling layer, there are usually large metal walls for power division, which can significantly affect the working bandwidth and the total profile of the multi-layered antenna arrays. Moreover, the multi-layered antenna

arrays are mainly fed with a uniform-amplitude distribution, which leads to high SLLs. For purpose of obtaining low sidelobe performance, 45° linearly polarized radiation units are developed. This method can optimize the radiation pattern without affecting the gain and the beam-width [25]. However, the overall SLL reduction is still limited, and moreover, this method usually requires an additional layer to adjust the radiation direction, making it difficult to be miniaturized.

The power division for the antenna array, which is mainly realized by the feeding network, can also dramatically affect the performance of the antenna array, especially its SLL [26]. Using unequal amplitude distribution can help to reduce the SLL. For instance, in complex antenna arrays, by using the Taylor distribution, the SLL can be suppressed due to the monotonic amplitude variation, realizing a good SLL [27]. However, it is more recommended to be used in a large antenna array where a large number of radiation elements is required [28]. For smaller antenna arrays, such as an 8-unit radiation structure, the Chebyshev distribution [29] can provide a similar power ratio to the Taylor distribution. While, for the same array size, the Chebyshev distribution can usually provide a lower SLL with the same beam-width. In order to realize the unequal power distribution by using either the Taylor or the Chebyshev distribution, T-junctions are necessarily designed for a waveguide-based feeding network. To reduce the unequal phases caused by the unequal power distribution in the T-junctions, some methods are developed. For instance, the width and the wall thickness at one of the outputs are often adjusted to compensate for the phase difference. Nevertheless, the adjustment range is very limited, especially for short or small T-junctions. Moreover, it is difficult to realize the impedance matching by using such structures for a complex full-corporate-feed network. For instance, the output port of the T-junction in the middle of the H-junction is often short [27]. As a result, a large width is required for high power distribution ratio, which is obviously difficult to achieve. This issue can be partly resolved by using the unequal T-junction power divider with phase compensation [28]. However, the two output ports are asymmetric, and thus, the design process will be also very complicated when it is used for a complex full-corporate-feed network.

In this paper, a wideband 16 × 16 slotted cavity waveguide-based antenna array is proposed for K-band applications. The main novelty of the developed study is that by introducing a high-order cavity mode ($TE_{220}$), a much more compact broadband antenna array is obtained. Another novelty is that, in order to provide unequal powers while keeping their phases the same, a simple and effective T-junction power divider structure is designed. Additionally, by properly designing the amplitude-tapering feeding network, based on the proposed T-junction power divider, a low SLL radiation pattern is obtained. The proposed topology is validated by using simulations based on the finite element method (FEM). The rest of the paper is organized as follows. In Section 2, the design principles of slotted cavity antenna array are presented, including the design of the subarray and the unequal T-junction-based feeding network. In Section 3, simulated results of the proposed 16 × 16 antenna array are discussed. The simulated results of the proposed antenna array are compared with the existing similar designs in the literature in Section 4. Finally, a conclusion is drawn in the final section.

## 2. Design of the Antenna Array

The configuration of the multi-layered corporate-fed 16 × 16 slotted cavity antenna array is shown in Figure 1. It consists of four parallel copper plates, i.e., the radiation slot layer, the cavity layer, the coupling aperture layer, and the feeding layer, which are denoted by "Layer1", "Layer2", "Layer3", and "Layer4", respectively. The 256 (16 × 16) radiation slots are regularly distributed in "Layer1", whose layout is particularly designed. The cavity layer "Layer2" consists of 8 × 8 square air cavities, which are used to excite the $TE_{220}$ mode [30] in the cavity. The coupling aperture layer "Layer3" is used to transmit the power from the feeding layer to the cavity layer. The feeding layer "Layer4" is designed

based on a rectangular waveguide, and is composed of 6-level cascading T-junctions so that electromagnetic waves can be transmitted to the coupling layer.

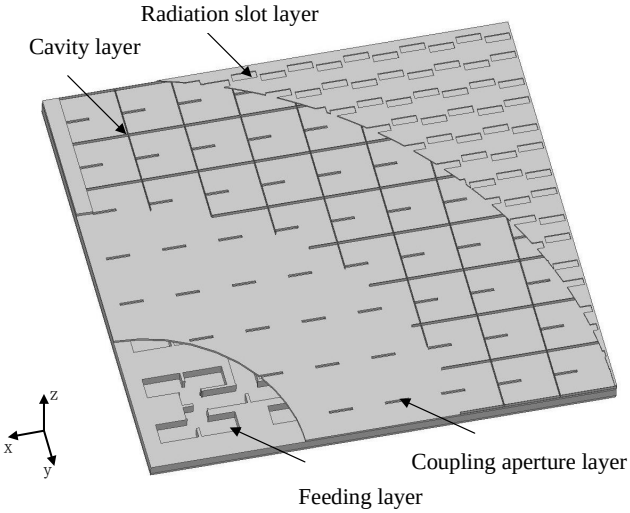


**Figure 1.** Overall configuration of the proposed waveguide-based multi-layered slotted cavity antenna array, which consists of four parallel copper plates: the radiation slot layer ("Layer1"), the cavity layer ("Layer2"), the coupling aperture layer ("Layer3"), and the feeding layer ("Layer4").

### *2.1. Basic 2 × 2-Slot Subarray*

Figure 2a presents a typical 2 × 2 radiating unit of the double-layer full-corporate-feed hollow-waveguide slotted antenna array [22].

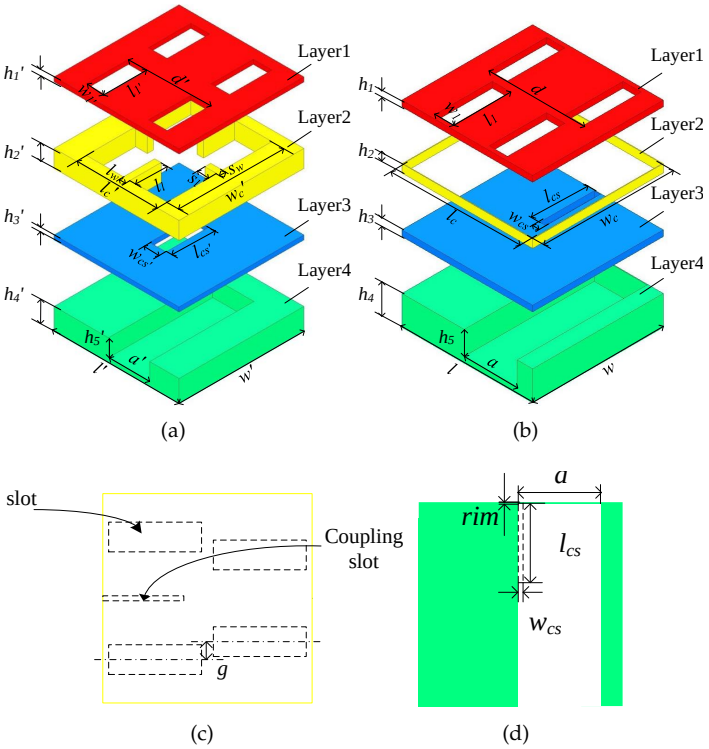


**Figure 2.** Configuration of (**a**) the primary and (**b**) the improved 2 × 2-slot subarrays, and the top views to show the detailed dimension relationship of the improved subarray (**c**) among "Layer1", "Layer2", and "Layer3" and (**d**) between "Layer3" and "Layer4".

According to the exploded perspective view of the primary 2 × 2-element subarray, the basic radiating unit consists of four radiation slots, an air-filled cavity, a plate with

a narrow coupling slot, and a part of the feeding network. Each layer is made of the same metal copper and has same sectional area (i.e., the same $w'$ and $l'$). To achieve good impedance matching, the designed thickness of each layer varies. As shown in Figure 2a, to optimize the radiation pattern, the four radiation slots in the primary subarray are evenly and symmetrically distributed in "Layer1". In order to minimize the grating lobes, the space between the slots ($d'$) is designed less than one free-space wavelength. The back cavity designed in "Layer2" has four large metal walls, which are designed to suppress unwanted higher modes. The coupling aperture is placed at the center of the "Layer3", and to realize a strong excitation in the cavity, it has an offset from the center axis of the waveguide in "Layer4", as illustrated in Figure 2a. Considering that the atmospheric propagation loss at lower frequencies of the K-band is smaller, the center frequency of the antenna herein designed focuses on 20 GHz.

It should be noted that the back cavity plays an important role in efficiently transmitting power from the coupling layer into the radiation slot layer. Thus, in order to optimize the radiation performance and to reduce the final profile, the back cavity is herein further improved by introducing the $TE_{220}$ mode, leading to an improved subarray as shown in Figure 2b. Figure 3 presents the $E$-field distribution of the $TE_{220}$ mode of the rectangular waveguide cavity in Figure 2b. It can be observed that there are four positions where the $E$-field has the maximum value, as denoted by "+" and "−" in Figure 3 to show the 180° phase difference of the $TE_{220}$ mode. The four red-dashed rectangles represent the designed $2 \times 2$ radiation slots of "Layer 1". It can be noted that the distances between the four slots are particularly designed, so that the radiated waves at the four slots are in phase. When the antenna works, the proposed cavity in "Layer2" performs as a resonance circuit. The relationship between the desired resonance frequency $f_{TE_{220}}$ and the cavity dimensions can be described by [2]:

$$f_{TE_{220}} = \frac{c}{2}\sqrt{\frac{4}{l_c^2} + \frac{4}{w_c^2}} \tag{1}$$

where $c$ represents the speed of light in free space, while $l_c$ and $w_c$ are the dimensions of the cavity in "Layer2" as shown in Figure 2b. The cavity is filled with air, and it is designed to excite the $TE_{220}$ mode at the center of the operating frequency (i.e., 20 GHz). Hence, $l_c$ and $w_c$ can be readily obtained by using Equation (1). To reduce the grating lobe, the distance between the radiation slots is designed less than one wavelength and the width of the radiation slot is designed less than one-quarter wavelength. Hence, the length $l$ and the width $w$ of the improved subarray are both $1.41\lambda_0$, where $\lambda_0$ is the free-space wavelength at the design frequency of 20 GHz. The dimensions of the proposed radiation unit in Figure 2b are listed in Table 1 in detail. The corresponding dimensions of Figure 2a are also provided by Table 1. Obviously, the cavity has been simplified, and the overall size, especially the height, of the subarray has been obviously reduced.

As presented in Figure 2c,d, the coupling slot in "Layer3" is designed right under the middle of the two distantly designed radiation slots, with the short edge close to the edge of "Layer2". The length $l_{cs}$ and the width $w_{cs}$ of the coupling slot are carefully designed, so that the desired $TE_{220}$ mode can be excited in the resonance cavity. In order to maximally transmit the power from "Layer4" to "Layer2", the edge of the feeding waveguide of "Layer4" is designed beneath the coupling slot of "Layer3", as shown in Figure 2d. The final design of the radiation unit is presented in Figure 2b and the corresponding dimension details are presented in Table 1 as well.

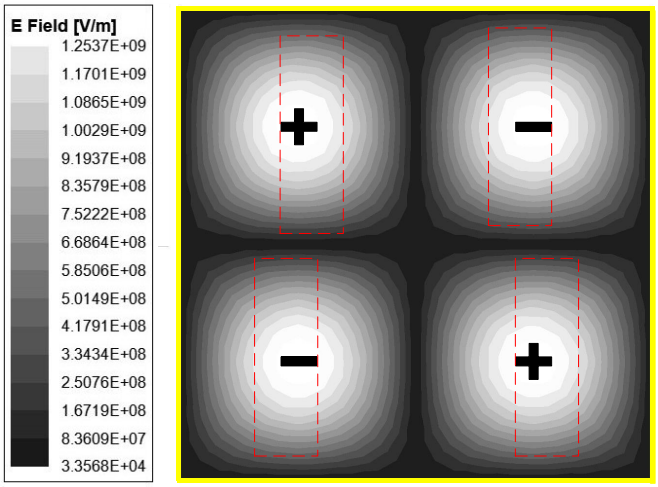


**Figure 3.** Amplitude distribution of the *E*-field for $TE_{220}$ mode in the cavity.

**Table 1.** Dimensions of the 2 × 2-element subarray (unit: mm).

| $h_1$ ($h_1'$) | $h_2$ ($h_2'$) | $h_3$ ($h_3'$) | $h_4$ ($h_4'$) | $h_5$ ($h_5'$) | $l$ ($l'$) | $w$ ($w'$) |
|---|---|---|---|---|---|---|
| 0.5 (0.9) | 1.33 (4.5) | 0.9 | 4.5 | 3.6 | 21.2 (26) | 21.2 (26) |
| $l_1$ ($l_1'$) | $l_l$ | $l_w$ | $s_l$ | $s_w$ | $w_1$ ($w_1'$) | $d$ ($d'$) |
| 9.32 (8.2) | 6.49 | 1.09 | 2.44 | 1.72 | 2.98 (3.28) | 16.54 |
| $l_c$ ($l_c'$) | $w_c$ ($w_c'$) | $l_{cs}$ ($l_{cs}'$) | $w_{cs}$ ($w_{cs}'$) | $a$ ($a'$) | $g$ | *rim* |
| 21 (16.28) | 21 (21.2) | 8.13 (8.96) | 0.5 (3.97) | 8.6 | 1.8 | 0.1 |

For comparison, the two radiation units shown in Figure 2a,b with the dimension information listed in Table 1, are analyzed by the ANSYS HFSS simulations. Figure 4 presents the reflection coefficients and the gains of the primary and the improved subarray units. It is noted that the reflection coefficient of the improved unit is always smaller than −15 dB in the frequency range from 17.6 GHz to 22.3 GHz (23.6%), while the corresponding bandwidth of the primary unit is from 18.4 GHz to 21.5 GHz (15.5%). Thus, the bandwidth of the proposed resonance cavity-based unit is much broader than the primary unit. The gain at the desired frequency 20 GHz is approximately 13.6 dBi for both the primary and the improved subarray units, which means that the introduced resonance cavity has almost no effect on the gain. The simulated radiation patterns of the two subarray units are presented in Figure 5. It is expected that the main lobe of the improved subarray in both *E*-plane and *H*-plane is located at 0°, indicating that the phases of the radiated waves through the four slots are the same. This is in a good agreement with the primary subarray unit. The 3 dB beam-width of the improved subarray unit is slightly larger (12.0% and 11.9% in *E*-plane and *H*-plane) compared to the primary subarray. The SLLs in the *E*-plane and the *H*-plane for the primary subarray are approximately −6.6 dB and −11.2 dB, respectively, whereas the corresponding *E*-plane and *H*-plane SLLs for the improved subarray are approximately −13 dB and −19 dB, respectively. This means that the improved subarray unit can provide a good SLL when it is used as a radiation antenna.

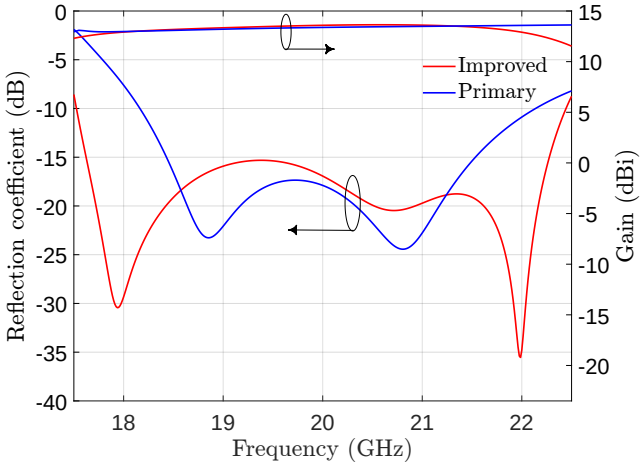


**Figure 4.** Simulated reflection coefficient and gain for the improved (red line) and primary (blue line) $2 \times 2$ subarrays.

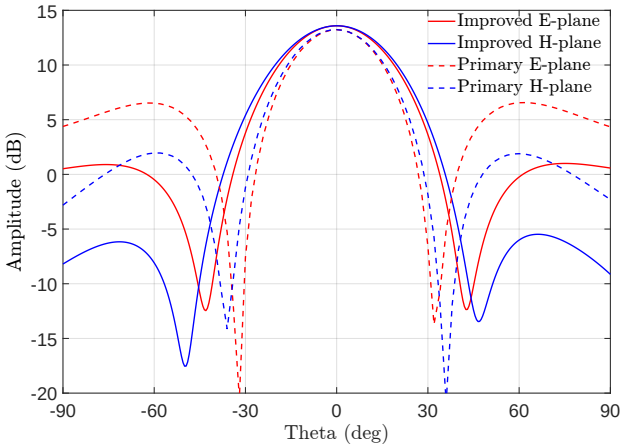


**Figure 5.** Radiation patterns for the improved (solid line) and primary (dashed line) $2 \times 2$ subarrays.

### *2.2. Power Feeding Network*

#### 2.2.1. Unequal Power Divider

In order to reduce the SLL, an unequal power dividing method is necessarily used to replace the amplitude-uniform feeding network [27]. The unequal power division is achieved by adding an offset metal wall and another two identical small metal windows in a T-junction. The offset metal wall is designed $m$ away from the middle of the input port (Port1), and the two windows are located at the end of the input port, as shown in Figure 6. By properly adjusting the location of the offset wall, a power division ratio as large as 7.31 dB between the two output ports (Port2 and Port3) can be achieved. Although a desired power ratio can be readily obtained by only adjusting the distance $m$ of the offset metal wall, there will also be an obvious phase difference between the two output waves. The phase difference can dramatically affect the final radiation performance of the antenna array. Therefore, the lengths $d_1$ and $d_2$ of the two outputs are changed to make the transmission paths of the two ports different, so that the phase difference between the two output ports can be compensated. This method can significantly improve the design flexibility and simplicity.

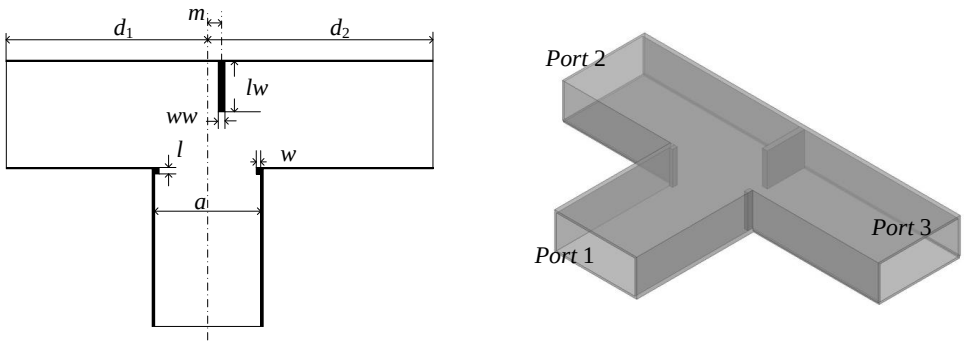


**Figure 6.** Unequal T-junction power divider ($a$ = 8.6 mm, $m$ = 0.97 mm, $l$ = 0.52 mm, $w$ = 0.36 mm, $lw$ = 4.08 mm, $ww$ = 0.54 mm, $d_1$ = 17.14 mm and $d_2$ = 17.46 mm).

The 6 dB unequal power divider shown in Figure 6 is simulated and the analytical results are plotted in Figure 7. It is seen that the reflection coefficient of the input port is always smaller than −25 dB, which indicates that a good impedance matching is achieved. Notably, an unequal power division at the two ports can be observed, and, as expected, the power ratio between Port2 and Port3 is 6 ± 0.9 dB within the frequency range from 17.5 GHz to 22.5 GHz. Additionally, the phase difference of the two outputs stays within ±0.8° over the entire operating bandwidth. These analytical results demonstrate that the proposed power division method can be used to freely design the power distribution in the complete feeding network, while keeping the output phase error within a minimum range.

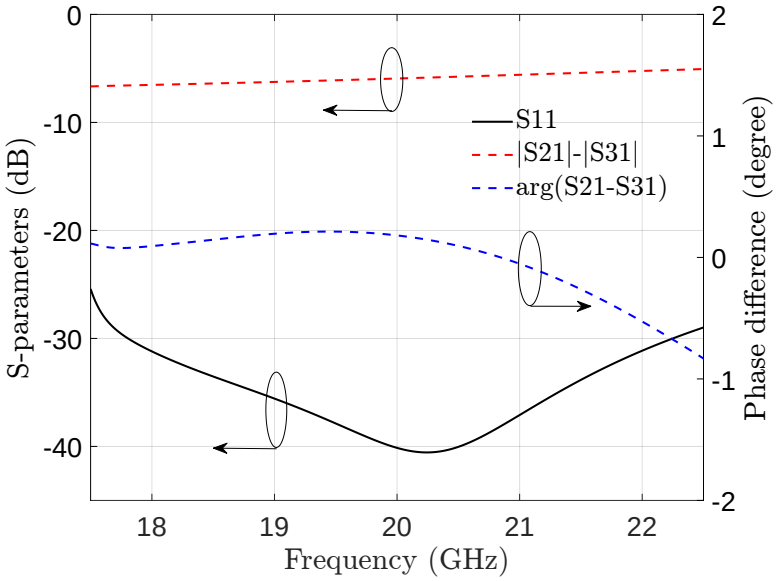


**Figure 7.** Simulated phase balance and S-parameters of the 6 dB power divider.

### 2.2.2. The Complete Feeding Network

A corporate-feed waveguide network is used in the 16 × 16 slotted antenna array. The number of output ports in $x$- and $y$-direction of the feeding network are both 8, and each port in the feeding network excites a subarray that consists of four radiating slots. The complete feeding network is designed symmetric in both $x$- and $y$-direction, as shown in the left of Figure 8. Hence, it can be divided into four repeating quarters, as illustrated in the right of Figure 8. In order to reduce the SLL of the final antenna array, the feeding network is carefully designed, so that a Chebyshev power distribution can be realized at each coupling slot in "Layer3". The Chebyshev power distribution is described by [31]

$$\sum_{i=1}^{N/2} I_i T_{2i-1}(x) = T_{N-1}(a_0 x) \quad (2)$$

where $I_i$ is the desired current in each output; $N$ is the number of the outputs; and $T(x)$ is the Chebyshev polynomial. The coefficient $a_0$ can be calculated with

$$a_0 = \frac{1}{2}\left[\left(R_0 + \sqrt{R_0^2 - 1}\right)^{\frac{1}{N-1}} + \left(R_0 + \sqrt{R_0^2 - 1}\right)^{-\frac{1}{N-1}}\right] \quad (3)$$

where $R_0$ can be calculated based on

$$R_{dB} = 20log\frac{1}{R_0} \quad (4)$$

In the designed feeding network, the port number $N$ is 8 and the Chebyshev synthesis $R_{dB}$ is expected to be −30 dB. Hence, according to Equation (2), the calculated normalized current amplitude of each unit is 0.26, 0.52, 0.82, 1, 1, 0.82, 0.52, and 0.26, respectively. By calculating the amplitude distribution, various T-junctions with different power ratios are obtained by changing the offset $m$ of the metal wall in the middle of the T-junction. The 6-level 1–64 power-weighted waveguide feeding network for the 16 × 16 slotted cavity antenna array is presented in Figure 8, with the detailed power ratios being given as well. As shown in Figure 8, four types of T-junctions that have different power ratios are designed, and the corresponding power ratios are 7.31 dB, 6 dB, 1.83 dB, and 0 dB, respectively.

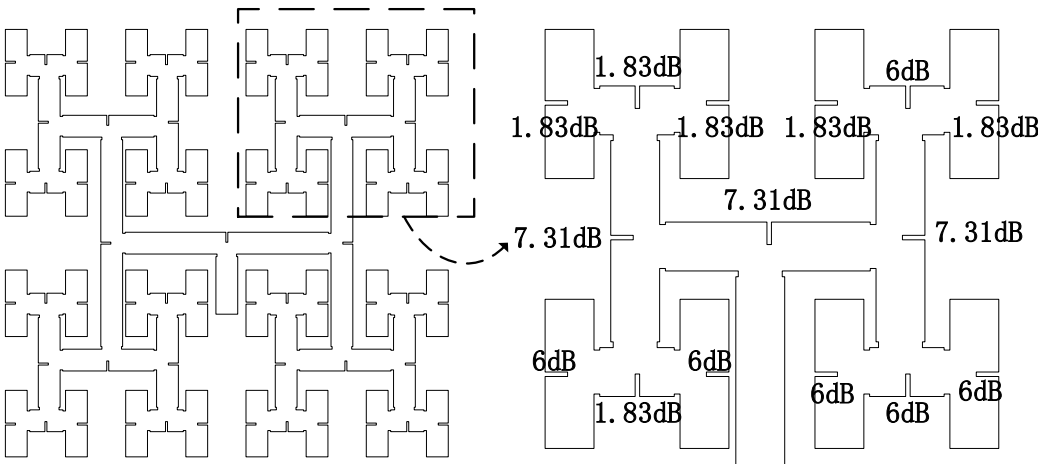


**Figure 8.** Power ratio required to achieve a quarter of the Chebyshev distribution.

## 3. Performance of the Proposed Antenna Array

With the regularly arrayed subarrays along the $x$- and $y$-axis, the whole antenna, which is fed by a 1–64 ways network, is obtained. The overall size of the final slotted cavity antenna array is 169.6 × 169.6 × 7.23 mm$^3$. The FEM simulation results of the reflection coefficient and the total gain are plotted in Figure 9. As can be seen in Figure 9, the reflection coefficient within the frequency range from 17.9 GHz to 22.3 GHz is always smaller than −10 dB, where the corresponding bandwidth is 21.9%. Several obvious ripples can be observed in the simulated reflection coefficient, which might be related to the multiple wave reflections in the long feeding network. Nevertheless, this has almost no effect on the radiation performance of the antenna array. Additionally, in the impedance bandwidth from 17.9 GHz to 22.3 GHz, the gain is always better than 28.1 dBi, and especially at the center frequency of 20 GHz, the peak gain is 29.1 dBi.

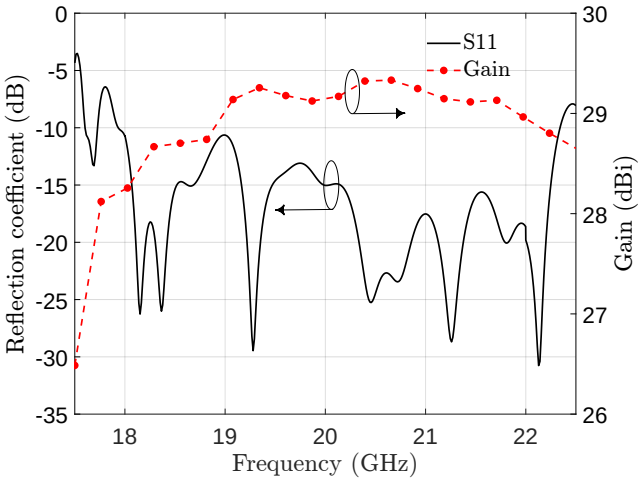


**Figure 9.** Reflection coefficient (black line) and gain (red line with symbols) for the proposed slotted cavity antenna array.

The simulated normalized radiation patterns in both *E*- and *H*-planes at arbitrary three frequency points of 17.9 GHz, 20 GHz, and 22.3 GHz are presented in Figure 10. There is a slight difference in the SLLs and the 3 dB beam-widths at the presented three frequencies for both the *E*-plane and the *H*-plane. For readability, the first SLLs and the 3 dB beam-widths at the three frequencies are listed in detail in Table 2. It is seen that, as expected, the maximum beam-widths appear at 18 GHz, and the corresponding values for *E*-plane and the *H*-plane are 6.82° and 7.23°, respectively. At the center frequency of 20 GHz, the 3 dB beam-widths for the *E*-plane and the *H*-plane are 5.46 deg and 5.74 deg, respectively.

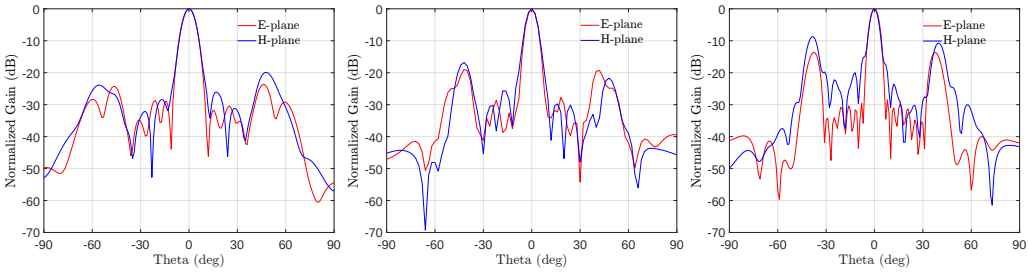


**Figure 10.** Normalized radiation patterns in the *E*-plane and *H*-plane at (**a**) 17.9 GHz, (**b**) 20 GHz, and (**c**) 22.3 GHz, respectively.

Obviously, the first SLLs in the *E*-plane at the three selected frequency points are close to the designed −30 dB, which demonstrates the good agreement between the simulated and theoretical results. Nevertheless, the first SLLs in the *H*-plane at the three frequency points are not as good as that in the *E*-plane, which might be related to the asymmetric distribution of the radiation slots in "Layer1" of Figure 1. Generally, at higher frequencies, both the first and the total SLLs are slightly larger. One reason is that with the decrease of the wavelength of the radiated waves, the grating lobes usually increase. Another reason is that at frequencies when the resonance cavity does not work at its resonant frequency, the phase difference of the radiated waves among the slots will increase, while at low frequencies, the phase difference can partly compensated by other modes, such as the $TE_{120}$ mode and the $TE_{210}$ mode of the resonance cavity. It can be further observed that there are two convex sidelobes at about $\theta = \pm 40°$ at the three frequencies, which might be related to the fact that the power distribution at the 16 × 16 radiation slots is not a typical Chebyshev distribution. As mentioned above, the power at the 8 × 8 coupling slots in "Layer3" is in Chebyshev distribution, while the waves at the four radiation slots of each subarray, which is supported by one coupling slot, are the same.

**Table 2.** Radiation characteristics of the proposed antenna.

| Frequency (GHz) | *E*-Plane HPBW (Degree) | *H*-Plane HPBW (Degree) | *E*-Plane First SLL (dB) | *H*-Plane First SLL (dB) |
|---|---|---|---|---|
| 17.9 | 7.01 | 6.87 | −28.9 | −26.1 |
| 20 | 5.46 | 5.74 | −28.3 | −24.8 |
| 22.3 | 4.94 | 4.69 | −28.5 | −20 |

## 4. Discussion

There are several types of antennas that can provide the radiation property of low sidelobe. The radiation performance of the proposed slotted cavity antenna array is compared to several typical antenna arrays in the literature. For a reliable and scientific comparison, simulation results from the literature are mainly listed in Table 3. Especially, the designed center frequency, working bandwidth, array scale, peak gain, first SLL, aperture efficiency, and the overall size are carefully compared. Due to the simplicity of implementation, microstrip antenna arrays [32–34] are mostly designed. The radiating units are uniformly distributed, with the impedance and the power distribution being controlled by adjusting the dimensions of the units and the series-fed network. As shown in Table 3, though a first SLL as small as −26.3 dB is achieved, the microstrip-based antenna array has a very limited working bandwidth. The Huygens antenna array [5] has a slightly broader bandwidth, and its bandwidth can be as large as 10% when it is designed as a 16 × 16 large-scale array by using a smaller compact feed network with tapered amplitude [35]. Especially, since it requires only a simple feeding network, its overall size can be designed slightly smaller. The SIW slot antenna array [7] can provide further better bandwidth and has slightly lower profile height, but its aperture efficiency is very low, due to its high dielectric loss. The dielectric resonator antenna array [29] can provide a much more enhanced bandwidth, as large as 31.9% and 38.1% for simulation and measurement results, respectively, by adjusting the dimensions of the feeding ring. However, it cannot achieve a low first SLL across the entire bandwidth, as its first SLL can be only obtained from 7.22 to 7.73 GHz (6.82%).

As can be seen from Table 3, slotted waveguide antenna arrays [19,27,28,36–38] can provide a relatively good balance between a wide bandwidth, a high gain, and a low sidelobe. As shown in Table 3, for a 16 × 16 antenna array that uses a uniform feeding network, the obtained SLL is only around −14 dB [19], which demonstrates that the proposed feeding network can dramatically reduce the SLL. However, as expected, using an unequal feeding network can slightly affect the aperture efficiency, especially when the array scale is large. The main part of the proposed antenna array is also based on slotted waveguide structure, but it involves a novel resonator cavity structure, which can particularly reduce the antenna size and enhance the bandwidth without affecting the gain. Therefore, as shown in Table 3, compared to most existing designs that use an unequal feeding network, the proposed antenna array can work in a sufficiently broad bandwidth, and especially, it has a comparably good first SLL and a high aperture efficiency. If the antenna arrays listed in Table 3 are all designed in the form of 16 × 16, the proposed improved slotted structure has almost the smallest dimensions. Even compared with the substrate-based antenna arrays [5,7,29], the proposed array has a comparable profile while having competitive first SLLs.

It should be noted that in the above discussion, only simulation results are compared. Obviously, there are usually some differences between simulated and measured results. To clarify the difference, all papers related to the proposed work in Table 3, especially some particular papers [19,27,28] are analyzed. A preliminary conclusion that the measured bandwidths have good agreements with (or are even better than [5,27–29]) the corresponding simulation results can be drawn. In addition, there is little difference (<2 dB) in the first SLL between the simulation and the measurement [7,27,28], while the simulated gain is only about 0.5 dB lower than the measured [5,7,19,28]. This means that the performance difference between simulation results and actual measurement results is very small [5,7,19,28],

which indicates that the simulation results can generally well reflect the actual performance of the antenna array. Therefore, the proposed slotted cavity antenna array is expected to feature wideband, low SLL, and high aperture efficiency in actual applications, if a proper fabrication process is used. In order to avoid the potential electromagnetic leakage, the proposed antenna array is planned to be fabricated by involving the additive manufacturing technology [39]. Though there are currently still some technical problems, a well-fabricated antenna can be expected in the near future. In addition, for wider applications, a suitable circular polarization is also planned in the near future. As the distance between the radiation slots in the proposed antenna array is very small, it is challenging to realize a general hexagonal radiating aperture [40]. Thus, a new circular polarization structure will be explored.

**Table 3.** Comparison of Previously Reported Antenna Arrays.

| Ref. | Center Frequency (GHz) | BW (%) | Scale | Peak Gain (dBi) | First SLL (dB) | Aperture Eff (%) | Size (Normalized to $\lambda_0$) |
|---|---|---|---|---|---|---|---|
| [33] | 9 | 1.6 | $1 \times 10$ | 15.6 | $-26.3$ | N/A | N/A |
| [5] | 10 | 4 | $4 \times 4$ | 18 | $-20$ | 72.7 | $2.92 \times 2.37 \times 0.25$ |
| [7] | 37.5 | 17.6 | $8 \times 8$ | 24..6 | $-18$ | 34.8 | $6.60 \times 6.60 \times 0.17$ |
| [29] | 7.5 | 31.9 | $1 \times 8$ | N/A | $-24.7$ | N/A | $1.05 \times 6.25 \times 0.24$ |
| [19] * | 60 | 20.3 | $16 \times 16$ | 33.7 | $\sim -14$ | 74.3 | $16.3 \times 15.44 \times 1.3$ |
| [27] | 15 | 12.6 | $16 \times 16$ | 30.2 | $-24.1$ | 58.7 | $12 \times 12 \times 0.73$ |
| [28] | 77 | 13.2 | $64 \times 32$ | 39.9 | $-20.2$ | 48.8 | $56.46 \times 28.23 \times 1.41$ |
| This work | 20 | 21.9 | $16 \times 16$ | 29.1 | $-22.5$ | 50.6 | $11.31 \times 11.31 \times 0.48$ |

* Based on a uniform feeding network.

## 5. Conclusions

A novel K-band slotted cavity antenna array is proposed, which has obvious advantages including wide bandwidth, low profile, and low SLL. The antenna consists of $16 \times 16$ slot antenna elements, which are fed by a Chebyshev power distribution-based 1–64 feeding network to realize the low SLL radiation performance. The Chebyshev power distribution is realized by using a series of unequal-power but equal-phase T-junctions. In order to reduce the complete profile, a simple shallow cavity, which works in the $TE_{220}$ mode, is designed. The high-order mode cavity is used to generate a resonance to efficiently transmit the power from the feeding network to the radiation slots. Based on the FEM simulation results, the proposed antenna array can provide a gain of 29.1 dBi at the desired center frequency of 20 GHz. Its 3 dB beam-widths in the *E*-plane and the *H*-plane are 5.46° and 5.74°, respectively, and its first SLLs in the *E*- and *H*-planes at 20 GHz are $-28.3$ dB and $-24.8$ dB, respectively. Compared to the existing similar studies, very good radiation performance including the aperture efficiency and the SLL is obtained by using the proposed antenna array. Due to the broad bandwidth and small size of the antenna array, it is ready to be integrated with other circuits and systems. Moreover, the design theories proposed in the paper can be used for developing other antennas to achieve very good radiation performance.

**Author Contributions:** Conceptualization, H.Y.; methodology, H.Y., J.L. and X.B.; theories, H.Y., Z.W. and M.B.L.; simulation analysis, H.Y. and Z.Z.; validation and data analysis, H.Y., G.G. and L.S.; writing—original draft preparation, H.Y., X.B. and G.C.; writing—review and editing, N.D., M.B.L. and G.C.; supervision, X.B. All authors have read and agreed to the published version of the manuscript.

**Funding:** The work is supported in part by the National Key R&D Program of China (Grant no. 2022YFF0604801), in part by the National Natural Science Foundation of China under Grant 62201037 and Grant 62271056, and in part by the BIT Youth Academic Start-up Funding XSQD-202206001.

**Data Availability Statement:** Not applicable.

**Acknowledgments:** The authors would like to acknowledge Zhuangzhuang Liu from the University of Science and Technology Beijing for the support in discussing the possibility and technologies for fabrication.

**Conflicts of Interest:** The authors declare no conflict of interest.

## Abbreviations

The following abbreviations are used in this manuscript:

| | |
|---|---|
| SLL | sidelobe level |
| SIW | substrate-integrated waveguide |
| FEM | finite element method |
| HPBW | half-power beamwidth |

## References

1. Jin, Y.; Chen, Y.; Ding, Y.; Zou, Z.; Qian, F.; Luo, Y.; Yang, G. A low-profile SIW-based CTS Array with reconfigurable four beams and dual polarizations for K-band sensing. *Sensors* **2022**, *22*, 3563. [CrossRef] [PubMed]
2. Li, W.; Da Xu, K.; Tang, X.; Yang, Y.; Liu, Y.; Liu, Q.H. Substrate integrated waveguide cavity-backed slot Array antenna using high-order radiation modes for dual-band applications in *K*-band. *IEEE Trans. Antennas Propag.* **2017**, *65*, 4556–4565. [CrossRef]
3. Lee, H.L.; Lim, W.G.; Oh, K.S.; Yu, J.W. 24 GHz balanced Doppler radar front-end with Tx leakage canceller for antenna impedance variation and mutual coupling. *IEEE Trans. Antennas Propag.* **2011**, *59*, 4497–4504. [CrossRef]
4. Jung, Y.B.; Eom, S.Y. Dual-band horn array design using a helical exciter for mobile satellite communication terminals. *IEEE Trans. Antennas Propag.* **2011**, *60*, 1336–1342. [CrossRef]
5. Lin, W.; Ziolkowski, R.W. Compact, highly efficient Huygens antenna array with low sidelobe and backlobe levels. *IEEE Trans. Antennas Propag.* **2021**, *69*, 6401–6409. [CrossRef]
6. Miao, K.; Zhang, Y.; Jing, H.; Wang, S.; Sun, H. Fast sidelobe calculation for planar phased arrays using an iterative sidelobe seeking method. *Electronics* **2022**, *11*, 3366. [CrossRef]
7. Jiang, X.; Jia, F.; Cao, Y.; Huang, P.; Yu, J.; Wang, X.; Shi, Y. Ka-band 8 × 8 low-sidelobe slot antenna array using a 1-to-64 high-efficiency network designed by new printed RGW technology. *IEEE Antennas Wirel. Propag. Lett.* **2019**, *18*, 1248–1252. [CrossRef]
8. Abulgasem, S.; Tubbal, F.; Raad, R.; Theoharis, P.I.; Liu, S.; Ali Khan, M.U. A wideband metal-only patch antenna for CubeSat. *Electronics* **2020**, *10*, 50. [CrossRef]
9. Hamberger, G.F.; Trummer, S.; Siart, U.; Eibert, T.F. A planar dual-polarized microstrip 1-D-beamforming antenna array for the 24-GHz band. *IEEE Trans. Antennas Propag.* **2016**, *65*, 142–149. [CrossRef]
10. Fang, D.G. *Antenna Theory and Microstrip Antennas*; CRC Press: Boca Raton, FL, USA, 2017.
11. Guan, D.F.; Ding, C.; Qian, Z.P.; Zhang, Y.S.; Guo, Y.J.; Gong, K. Broadband high-gain SIW cavity-backed circular-polarized array antenna. *IEEE Trans. Antennas Propag.* **2016**, *64*, 1493–1497. [CrossRef]
12. Liu, J.; Jackson, D.R.; Long, Y. Substrate integrated waveguide (SIW) leaky-wave antenna with transverse slots. *IEEE Trans. Antennas Propag.* **2011**, *60*, 20–29. [CrossRef]
13. Bao, X.; Wang, L.; Wang, Z.; Zhang, J.; Zhang, M.; Crupi, G.; Zhang, A. Simple, fast, and accurate broadband complex permittivity characterization algorithm: Methodology and experimental validation from 140 GHz up to 220 GHz. *Electronics* **2022**, *11*, 366. [CrossRef]
14. Bao, X.; Liu, S.; Ocket, I.; Bao, J.; Schreurs, D.; Zhang, S.; Cheng, C.; Feng, K.; Nauwelaers, B. A general line-line method for dielectric material characterization using conductors with the same cross-sectional geometry. *IEEE Microw. Wirel. Compon. Lett.* **2018**, *28*, 356–358. [CrossRef]
15. Sakakibara, K.; Kimura, Y.; Akiyama, A.; Hirokawa, J.; Ando, M.; Goto, N. Alternating phase-fed waveguide slot arrays with a single-layer multiple-way power divider. *IEE Proc.-Microwaves Antennas Propag.* **1997**, *144*, 425–430. [CrossRef]
16. Hirokawa, J.; Zhang, M.; Ando, M. 94 GHz Fabrication of a Slotted Waveguide Array Antenna by Diffusion Bonding of Laminated Thin Plates. In Proceedings of the SENSORS, 2009 IEEE, Christchurch, New Zealand, 25–28 October 2009; pp. 907–911.
17. Ettorre, M.; Manzillo, F.F.; Casaletti, M.; Sauleau, R.; Le Coq, L.; Capet, N. Continuous transverse stub array for Ka-band applications. *IEEE Trans. Antennas Propag.* **2015**, *63*, 4792–4800. [CrossRef]
18. Chairi, Y.; Abedrrabba, S.; Allanic, R.; Amiaud, A.C.; El Oualkadi, A.; Quendo, C.; Merlet, T.; Reklaoui, K.; Le Gouguec, T. Design of a slotted waveguide antenna based on TE20 mode in Ku-band suitable for direct metal laser sintering. *Electronics* **2022**, *11*, 2079. [CrossRef]
19. Ji, S.; Hirokawa, J.; Tomura, T. A wideband and high-gain all-metallic perpendicular-corporate-fed multi-layered parallel-plate slot array antenna. *IEEE Access* **2022**, *10*, 38000–38011. [CrossRef]
20. Casula, G.A.; Mazzarella, G.; Montisci, G.; Muntoni, G. A review on improved design techniques for high performance planar waveguide slot arrays. *Electronics* **2021**, *10*, 1311. [CrossRef]

21. Park, S.; Tsunemitsu, Y.; Hirokawa, J.; Ando, M. Center feed single layer slotted waveguide array. *IEEE Trans. Antennas Propag.* **2006**, *54*, 1474–1480. [CrossRef]
22. Miura, Y.; Hirokawa, J.; Ando, M.; Shibuya, Y.; Yoshida, G. Double-layer full-corporate-feed hollow-waveguide slot array antenna in the 60-GHz band. *IEEE Trans. Antennas Propag.* **2011**, *59*, 2844–2851. [CrossRef]
23. Tekkouk, K.; Hirokawa, J.; Oogimoto, K.; Nagatsuma, T.; Seto, H.; Inoue, Y.; Saito, M. Corporate-feed slotted waveguide array antenna in the 350-GHz band by silicon process. *IEEE Trans. Antennas Propag.* **2016**, *65*, 217–225. [CrossRef]
24. Zarifi, D.; Farahbakhsh, A.; Zaman, A.U.; Kildal, P.S. Design and fabrication of a high-gain 60-GHz corrugated slot antenna array with ridge gap waveguide distribution layer. *IEEE Trans. Antennas Propag.* **2016**, *64*, 2905–2913. [CrossRef]
25. Tomura, T.; Hirokawa, J.; Hirano, T.; Ando, M. A 45° Linearly polarized hollow-waveguide 16 × 16-slot array antenna covering 71–86 GHz band. *IEEE Trans. Antennas Propag.* **2014**, *62*, 5061–5067. [CrossRef]
26. Nguyen, D.H.; Ala-Laurinaho, J.; Moll, J.; Krozer, V.; Zimmer, G. Improved sidelobe-suppression microstrip patch antenna array by uniform feeding networks. *IEEE Trans. Antennas Propag.* **2020**, *68*, 7339–7347. [CrossRef]
27. Huang, G.L.; Zhou, S.G.; Chio, T.H.; Hui, H.T.; Yeo, T.S. A low profile and low sidelobe wideband slot antenna array feb by an amplitude-tapering waveguide feed-network. *IEEE Trans. Antennas Propag.* **2014**, *63*, 419–423. [CrossRef]
28. Qin, L.; Lu, Y.; You, Q.; Wang, Y.; Huang, J.; Gardner, P. Millimeter-wave slotted waveguide array with unequal beamwidths and low sidelobe levels for vehicle radars and communications. *IEEE Trans. Veh. Technol.* **2018**, *67*, 10574–10582. [CrossRef]
29. Lin, J.; Shen, W.; Yang, K. A low-sidelobe and wideband series-fed linear dielectric resonator antenna array. *IEEE Antennas Wirel. Propag. Lett.* **2016**, *16*, 513–516. [CrossRef]
30. Han, W.; Yang, F.; Long, R.; Zhou, L.; Yan, F. Single-fed low-profile high-gain circularly polarized slotted cavity antenna using a high-order mode. *IEEE Antennas Wirel. Propag. Lett.* **2016**, *15*, 110–113. [CrossRef]
31. Hansen, R.C. *Phased Array Antennas*; John Wiley & Sons: Hoboken, NJ, USA, 2009.
32. Kothapudi, V.K. SFCFOS uniform and Chebyshev amplitude distribution linear array antenna for K-band applications. *J. Electromagn. Eng. Sci.* **2019**, *19*, 64–70. [CrossRef]
33. Yin, J.; Wu, Q.; Yu, C.; Wang, H.; Hong, W. Low-sidelobe-level series-fed microstrip antenna array of unequal interelement spacing. *IEEE Antennas Wirel. Propag. Lett.* **2017**, *16*, 1695–1698. [CrossRef]
34. Nikkhah, M.R.; Rashed-Mohassel, J.; Kishk, A. A low sidelobe and wideband series-fed dielectric resonator antenna array. In Proceedings of the 2013 21st Iranian Conference on Electrical Engineering (ICEE), Mashhad, Iran, 14–16 May 2013; IEEE: Piscataway, NJ, USA, 2013; pp. 1–3.
35. Lin, W.; Ziolkowski, R.W. Ka-band huygens antenna array with very high aperture efficiency and low sidelobes. *IEEE Trans. Antennas Propag.* **2022**, *Early Access*. [CrossRef]
36. Ran, J.; Jin, C.; Zhang, P.; Wang, W.; Wu, Y. High-gain and low-Loss dual-polarized antenna array with reduced sidelobe level based on gap waveguide at 28 GHz. *IEEE Antennas Wirel. Propag. Lett.* **2022**, *21*, 1022–1026. [CrossRef]
37. Shen, R.; Ye, X.; Xie, J.; Chen, Z.; Jin, C. A W-band circular box-horn antenna array radiating sum and difference beams with suppressed sidelobe. *IEEE Trans. Antennas Propag.* **2019**, *67*, 5934–5942. [CrossRef]
38. Wang, Y.; Tan, W.; Zhu, K.; Luo, H.; Zhao, G.; Sun, H. Design of a Ka-band 3D-printed dual-polarization magnetoelectric dipole antenna array with low sidelobe. *Electronics* **2021**, *10*, 2969. [CrossRef]
39. Li, Y.; Ge, L.; Wang, J.; Da, S.; Cao, D.; Wang, J.; Liu, Y. 3-D printed high-gain wideband waveguide fed horn antenna arrays for millimeter-wave applications. *IEEE Trans. Antennas Propag.* **2019**, *67*, 2868–2877. [CrossRef]
40. Miura, Y.; Hirokawa, J.; Ando, M.; Igarashi, K.; Yoshida, G. A circularly-polarized aperture array antenna with a corporate-feed hollow-waveguide circuit in the 60 GHz-band. In Proceedings of the 2011 IEEE International Symposium on Antennas and Propagation (APSURSI), Spokane, WA, USA, 3–8 July 2011; IEEE: Piscataway, NJ, USA, 2011; pp. 3029–3032.